Single-crystal elasticity of the rhodochrosite at high pressure by Brillouin scattering spectroscopy

Chaoshuai Zhao, Heping Li, Pofei Chen, Jianjun Jiang & Wen Liang

Published online: 13 Jul 2018.

Submit your article to this journal ✎

View Crossmark data

Taylor & Francis
Taylor & Francis Group

Check for updates

Single-crystal elasticity of the rhodochrosite at high pressure by Brillouin scattering spectroscopy

Chaoshuai Zhao[a,b], Heping Li[a], Pofei Chen[c], Jianjun Jiang[a] and Wen Liang[a]

[a]Key Laboratory of High-temperature and High pressure Study of the Earth's Interior, Institute of Geochemistry, Chinese Academy of Sciences, Guiyang, People's Republic of China; [b]College of Earth Sciences, University of Chinese Academy of Sciences, Beijing, People's Republic of China; [c]Department of Earth Sciences, National Central University, Taoyuan, Taiwan

ABSTRACT

The sound velocity properties of single-crystal rhodochrosite ($MnCO_3$) were determined up to 9.7 GPa at ambient temperature by Brillouin scattering spectroscopy. Six elastic constants were calculated by a genetic algorithm method using the Christoffel's equations at each pressure. The elastic constants increased linearly as a function of pressure and its pressure derivatives $\partial Cij/\partial P$ for C_{11}, C_{33}, C_{44}, C_{12}, C_{13}, C_{14} were 5.86 (±0.36), 3.82 (±0.44), 2.06 (±0.39), 5.07 (±0.27), 5.34 (±0.44), 1.52 (±0.24), respectively. Based on the derived elastic constants of rhodochrosite, the aggregate adiabatic bulk and shear moduli (K_s and G) were calculated using the Voigt-Reuss-Hill averages and the linear fitting coefficients $(\partial K_s/\partial P)_T$ and $(\partial G/\partial P)_T$ were 5.05(±0.26) and 0.73 (±0.05), respectively. The aggregate V_p of rhodochrosite increased clearly as a function of pressure and its pressure derivative $\partial V_p/\partial P$ was 7.99(±0.53) × 10^{-2} km/(s GPa), while the aggregate V_s increased slowly and $\partial V_s/\partial P$ was only 1.19(±0.12) × 10^{-2} km/(s GPa). The anisotropy factor for As of rhodochrosite increased from ~40% at 0.8 GPa to ~48% at 9.7 GPa, while A_p decreased from ~19% to ~16% at the corresponding pressure.

1. Introduction

Carbonates play an important role in the transport and storage of carbon in the Earth's interior [1,2]. The most important carbonate minerals belonging to the calcite group, include calcite ($CaCO_3$), magnesite ($MgCO_3$), rhodochrosite ($MnCO_3$), siderite ($FeCO_3$) [3]. Calcite, magnesite, and siderite are widely studied as the most important carbon carriers of carbonates in the crust and mantle [4–6]. Rhodochrosite is reported as a potential carbon-bearing phase for transporting the carbon into the Earth's deep interior [7]. It appears most commonly in hydrothermal ore districts [3] and its high pressure phase is stable to lower mantle conditions [7,8]. In addition, Mn^{2+} has a cation size close to Mg^{2+} and Fe^{2+}, which could make rhodochrosite a potential model compound for understanding the difference in the high pressure behaviors of magnesite and siderite [9]. However, the study of rhodochrosite is mainly concentrated on the vibration and compressibility

properties previously [7,8], its sound velocities and elastic properties are little reported and limited at 1 GPa and ambient temperature [10,11]. Therefore, we investigated the high pressure velocity of rhodochrosite up to 9.7 GPa at ambient temperature by Brillouin scattering here.

2. Experiments

Natural samples of rhodochrosite were obtained from Guizhou, China. The composition was measured by electron microprobe analyses (JXA-8230, 15 kV and 10 nA, Northwest University, China), which indicated a homogeneous chemical composition of $MnCO_3$ with a minor Fe, Ca and Mg and its composition was $(Mn_{0.976}Fe_{0.011}Ca_{0.003}Mg_{0.001})CO_3$. For simplification, we referred it to $MnCO_3$ thereafter. The single-crystal samples were cleaved using a tungsten needle along the rhombohedral cleavage parallel to (101) plane. Optically transparent, surfaces with a parallelism better than 30′ single-crystal samples were chosen for preparation, then an appropriate size of the single-crystal sample was carefully cut and loaded into a diamond anvil cell (DAC) with a tungsten needle for Brillouin scattering measurement. When an incident white light was upon the sample, it produced a wedge interference pattern between the sample lower surface and the lower diamond upper surface. The parallelism was checked by microscope through observing the interference stripe and the situation with many interference stripes was discarded. The parallelism α between the sample and diamond surfaces is defined as follows:

$$\alpha \approx \frac{180\lambda}{2nd\pi}(°) \tag{1}$$

where λ is the wavelength of incident light (~535 nm for green light), n is the refractive index of the pressure transmitting medium (~1.3), d is the distance between the adjacent interference stripes (~25 μm). Based on the calculation of the Equation (1), we obtained that the value of α was ~0.5°.

High pressure was generated by a cell with two opposed diamonds with 400 μm culets. The initial thickness of rhenium gasket was pre-indented to ~70 μm. A 4:1 volume ratio of methanol and ethanol mixture was applied as the pressure transmitting medium. Ruby powders and a single-crystal chip of rhodochrosite were placed in a ~150 μm sample chamber. The sample size was 77 μm × 62 μm × 40 μm. The pressure was determined by the quasi-hydrostatic ruby scale [12]. In this study, the uncertainty of pressure ranged over ±0.1~0.2 GPa, which was estimated from a difference between the pressure measured before and after the collection of the Brillouin spectrum.

The diagram of the experimental setup was similar to Zha et al. [13]. The main component of the Brillouin scatting system consisted of a diode-pumped laser with a wavelength of 532 nm (Verdi G2, Coherent Company), a Sandercock-type six-pass tandem Fabry–Perot interferometer (TFP2, JRS Scientific Instruments) and a spectrum collection system. More detailed information about the component can be seen from Murakami et al. [14]. In this measurement system, a DAC mounted on the multi-axial stage (Edmund Optics, Newport and Parker Company) with $XYZ\theta\chi\alpha$ was placed on the corner with 120° angle optical path system. The sample chamber was observed through an Olympus microscope with a 20× ultra-length working distance objective along the laser

exit orientation. A symmetric 60° scattering geometry was adopted in all experiments. This geometry was calibrated before experiments by using BK7 glass and H_2O [15,16]. The incident laser power was 150 mW. A 300 μm incident pinhole at the front of the interferometer and a 450 μm exit pinhole at the front of CCD signal collection system were used to collect the sample signal. Before each experiment, we calibrated the spectrum range of Brillouin scattering.

In the symmetric scattering geometry, the acoustic velocity, proportional to the Brillouin frequency shift, was calculated as follows [17]:

$$V_i = \frac{\Delta \omega_i \lambda}{2 \sin (\theta/2)},$$

(2)

where V_i is the velocity of an acoustic wave (subscript i stands for the longitudinal or transversal mode), $\Delta\omega_i$ is the frequency shift of scattered light and λ (532 nm) is the wavelength of the incident light, θ (60°) is the angle between incident and scattered orientation.

3. Results and discussion

Brillouin scattering spectra of single-crystal rhodochrosite were determined up to 9.7 GPa at ambient temperature in a 1–2 GPa pressure interval. The spectra were collected in the (101) plane in 19 different crystallographic directions at 10 degree interval for each pressure. The intensity of V_p and V_s varied with the change of different crystallographic directions. A representative Brillouin spectrum of $MnCO_3$ at 8.6 GPa and 300 K was shown in Figure 1. At the pressure below 3.1 GPa, some transverse velocities V_s were not detected due to the sample signal overlapping with the pressure transmitting medium at some crystallographic directions. At 7.3 GPa, the signal of pressure transmitting medium was not detected, which was good for collecting better sample signals. It should be noted that rhodochrosite has a property of birefringence. The extraordinary ray does
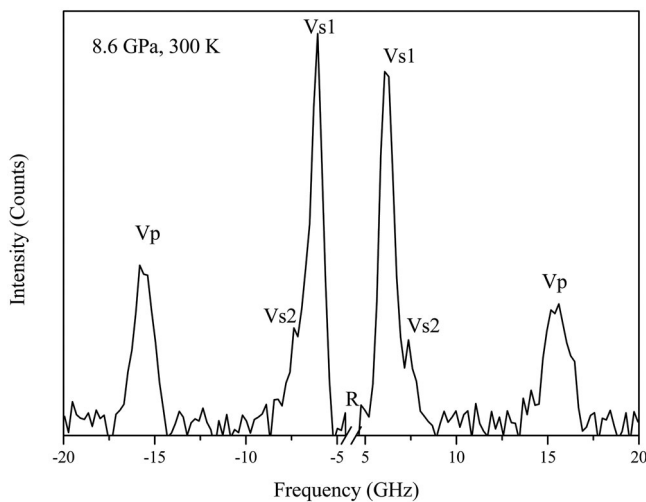

Figure 1. Representative Brillouin spectrum of single-crystal rhodochrosite at 8.6 GPa and 300 K. R: Rayleigh peak.

not follow Snell's law and the velocity of this orientation cannot be calculated by the Equation (1) [18]. However, the difference in frequency shift between ordinary and extra-ordinary rays is estimated to be 2% or less [10], which is almost less than or equal to the resolution of the Brillouin scattering system. Therefore, for simplification, the effect of the extraordinary ray to the velocity of rhodochrosite is neglected in this study.

The representative V_p and V_s velocities of single-crystal rhodochrosite as a function of the azimuthal angle at 8.6 GPa and 300 K were shown in Figure 2. The change of V_p and V_s as a function of the azimuthal angle was clearly observed, which indicated strong elastic anisotropies of the sample at high pressure. The phenomenon is well in agreement with the result of rhodochrosite at ambient temperature and ambient pressure [10]. Some other carbonates, such as magnesite and magnesiosiderite (($Fe_{0.65}Mg_{0.35}$)CO_3), also show the similar results before the phase transition [19,20], which are different from aragonite-type of strontianite ($SrCO_3$) and aragonite ($CaCO_3$) [21,22]. The similar change of velocities as a function of the azimuthal angle for rhodochrosite, magnesite, and magne-siosiderite is likely due to them belonging to the same calcite group and having the similar characteristics.

Based on the 19 sets of V_p, V_{s1} and, V_{s2} at each pressure, the six elastic constants of rho-dochrosite were calculated by a genetic algorithm method using the Christoffel's equations with initial densities from an equation of state of rhodochrosite [23,24]. The method has been successfully applied to invert the elastic constants of Zn(2-methylimidazolate)$_2$ (zeolitic imidazolate framework), magnesite, and dolomite [23,25]. In addition, the elastic constants of the rhodochrosite at ambient conditions were recalcu-lated based on the velocities and density previously reported [10]. Compared with the results calculated by this method and references reported, the errors for most elastic con-stants are within ~1% except that C_{13} and C_{33} are ~3%, which further proves the reliability of this method.
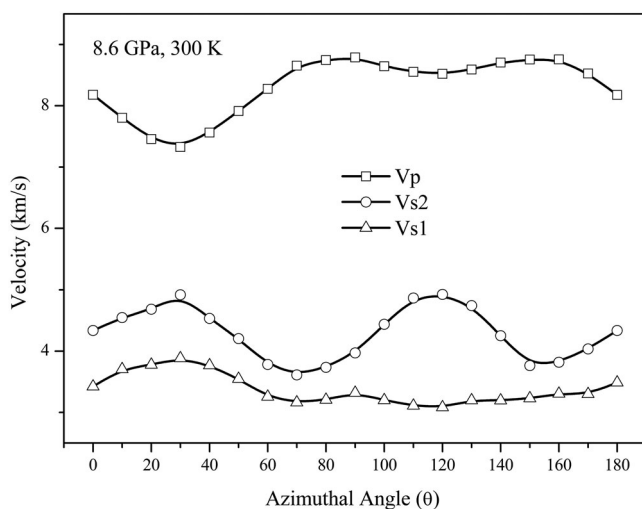

Figure 2. V_p and V_s velocities of single-crystal rhodochrosite as a function of the azimuthal angle at 8.6 GPa and 300 K.

The uncertainty for each elastic constant was estimated by calculating the variations of the misfit as a function of the specific Cij, more detailed information could be seen from Chen et al. [23]. The maximum errors of the elastic constants for C_{11}, C_{33}, C_{44}, C_{12}, C_{13}, C_{14} are 0.9%, 4.1%, 3.1%, 2.7%, 3.4% and 6.1% respectively within whole pressure range based on the results from this study. These errors should be related to density and sound velocity. On the one hand, due to the shortage of in situ single-crystal X-ray diffraction data of the sample in this study, the density is calculated by the equation of state of previous study, which should lead to a little difference between the calculated density and real one, further leading to a little calculation error of the elastic constants. On the other hand, parallelism, birefringence and pressure transmitting medium all affect the accuracy of the sound velocity, which further affects the accurate calculation of the elastic constants. Firstly, the error of sound velocity caused by parallelism comes from two parts, one is between the sample lower surface and the lower diamond upper surface, and the other is between the sample upper and lower surfaces. Both cases imply that the parallelism of 0.5° results in 0.4% velocity error according to the calculation equations from reference reported by Zha et al. (see the case 1 and case 2 in the reference's appendix) [13]. Therefore, the velocity error is ≤0.8% for angles errors ≤1°. Secondly, the effect of birefringence can bring about ≤2% error of the sound velocity. Thirdly, at pressure below 3.1 GPa, the sample signals overlapping with pressure transmitting medium at some crystallographic directions can give rise to the uncertainty of the sound velocity.

The representative elastic constants of rhodochrosite as a function of pressure were shown in Figure 3 and Table 1. Each of the elastic constants increased almost linearly as a function of pressure and the pressure derivatives of the elastic constants $\partial Cij/\partial P$ for C_{11}, C_{33}, C_{44}, C_{12}, C_{13}, C_{14} were 5.86 (±0.36), 3.82 (±0.44), 2.06 (±0.39), 5.07 (±0.27), 5.34 (±0.44), 1.52 (±0.24), respectively. The derived elastic constants at ambient conditions are in agreement with previous results within experimental errors [10]. The cationic radius exhibits the relationship as follows: $r(Mn^{2+}) > r(Fe^{2+}) > r(Mg^{2+})$, for the same calcite-type divalent metal carbonates MCO_3 ($M = Mg^{2+}$, Fe^{2+}, Mn^{2+}), in general, the larger the cationic radius, the weaker the interatomic interactions potential, which can lead to a series of change of the mineral, such as structural, elastic, velocities, and thermodynamic properties, etc. [26]. Compared with the elastic constants of rhodochrosite and magnesite at high pressure and ambient temperature, the three diagonal elastic constants C_{11}, C_{33}, C_{44} of the former are all less than the latter [20]. It can be explained as a weakening of the longitudinal elastic coefficients due to the weakening of interatomic interactions potential of the rhodochrosite, which is also proved by other carbonates like calcite, strontianite and aragonite at ambient conditions [10,21]. The relationship is not suitable for siderite no matter at ambient conditions or high pressure, which can be explained as a crystal field stabilization of Fe^{2+} [27].

Using the derived elastic constants of rhodochrosite, the aggregate adiabatic bulk and shear moduli (K_s and G) were calculated by the Voigt-Reuss-Hill averages [28] and the linear fitting coefficients $(\partial K_s/\partial P)_T$ and $(\partial G/\partial P)_T$ were 5.05 (±0.26) and 0.73 (±0.05), respectively (see Figure 4). The derived bulk and shear moduli (K_0 and G_0) at ambient conditions are 108.5 (±1.8) and 50.6 (±0.3) GPa respectively, which is in agreement with previous results [10]. Based on the aggregate adiabatic bulk and shear moduli, the aggregate V_p
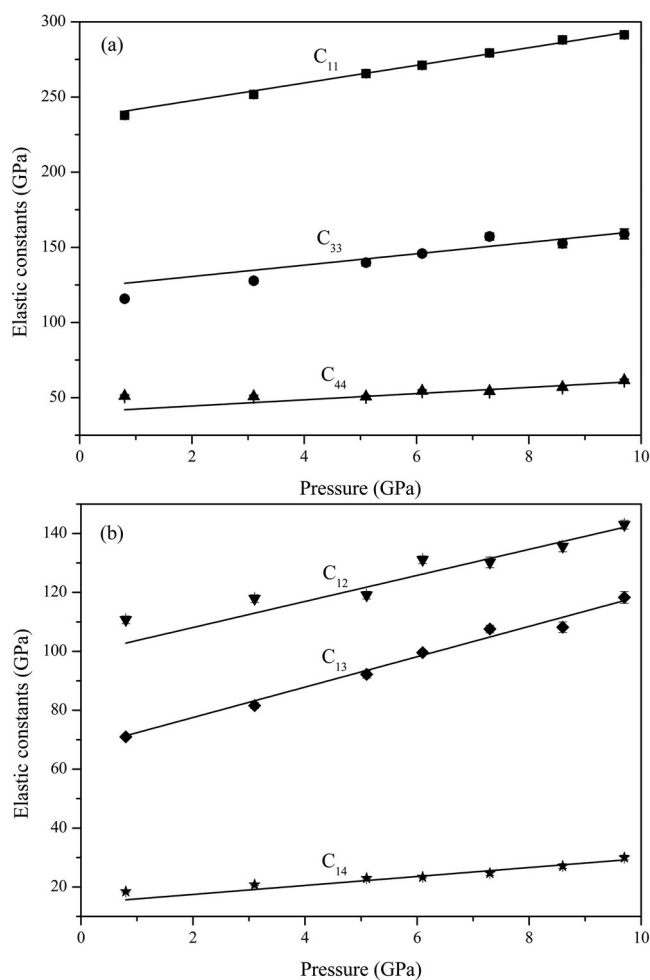
Figure 3. Elastic constants of rhodochrosite as a function of pressure at ambient temperature.

Table 1. Representative elastic properties of rhodochrosite at high pressure and ambient temperature.

| P (GPa)	5.1 (±0.2)	6.1 (±0.2)	7.3 (±0.1)	8.6 (±0.2)	9.7 (±0.1)
C_{11} (GPa)	265.6 (±1.5)	271.1 (±1.5)	279.3 (±2.5)	288.0 (±2.5)	291.4 (±1.5)
C_{33} (GPa)	139.8 (±4.0)	145.9 (±3.0)	157.2 (±4.5)	152.6 (±5.5)	158.9 (±6.5)
C_{44} (GPa)	50.6 (±1.5)	54.4 (±1.5)	54.2 (±1.5)	56.9 (±1.5)	61.5 (±1.5)
C_{12} (GPa)	119.1 (±2.5)	131.1 (±2.5)	130.2 (±3.5)	135.6 (±3.5)	143.0 (±3.0)
C_{13} (GPa)	92.2 (±2.5)	99.6 (±1.5)	106.6 (±2.5)	110.2 (±3.5)	118.3 (±4.0)
C_{14} (GPa)	23.0 (±0.5)	23.4 (±0.5)	24.7 (±1.5)	27.1 (±1.5)	30.0 (±1.5)
K_s (GPa)	133.2 (±2.3)	140.6 (±1.9)	147.9 (±3.0)	150.1 (±3.5)	157.0 (±3.7)
G (GPa)	54.4 (±2.0)	55.0 (±2.0)	56.3 (±2.8)	57.0 (±3.0)	57.2 (±2.9)
V_p (km/s)	7.31 (±0.09)	7.42 (±0.08)	7.55 (±0.11)	7.56 (±0.13)	7.67 (±0.12)
V_s (km/s)	3.76 (±0.02)	3.77 (±0.02)	3.79 (±0.03)	3.80 (±0.03)	3.80 (±0.02)
A_p (%)	17.8	18.5	18.3	18.0	16.2
A_{smax} (%)	44.8	43.3	46.6	48.4	47.8
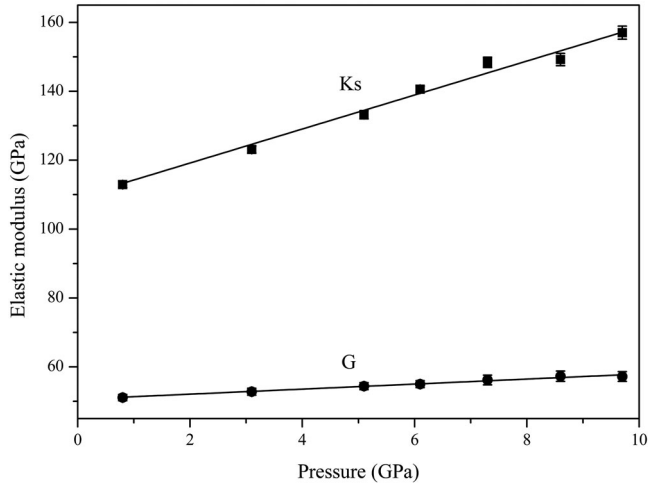
Figure 4. Adiabatic bulk and shear moduli of rhodochrosite as a function of pressure at ambient temperature.

and V_s of rhodochrosite were calculated by the following equations:

$$V_p = \sqrt{\frac{K_s + (4/3)G}{\rho}},$$ (3)

$$V_s = \sqrt{\frac{G}{\rho}},$$ (4)

The aggregate V_p of rhodochrosite increased clearly and linearly as a function of pressure and its pressure derivatives $\partial V_p / \partial P$ was $7.99(\pm 0.53) \times 10^{-2}$ km/(s·GPa), while the aggregate
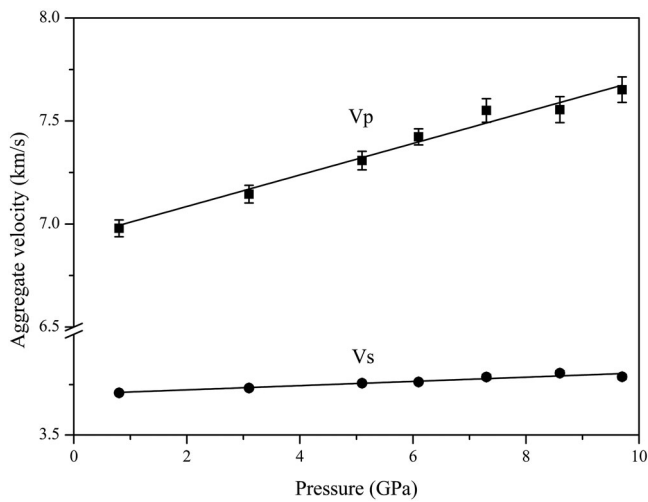

Figure 5. Aggregate compressional and shear velocities of rhodochrosite as a function of pressure at ambient temperature.

V_s of rhodochrosite increased slowly and $\partial V_s/\partial P$ was only $1.19(\pm 0.12) \times 10^{-2}$ km/(s·GPa) (see Figure 5).

The derived anisotropy factors for A_p (V_p) and A_s (V_s) of the rhodochrosite were exhibited at Figure 6. The anisotropy factor for A_p (V_p) is defined as:

$$A_p = 2 \times (V_{p,max} - V_{p,min})/(V_{p,max} + V_{p,min}) \times 100\%, \quad (5)$$

where $V_{p,max}$ and $V_{p,min}$ represent the maximum and minimum compressional wave velocities of the mineral, respectively. The anisotropy factor for A_s (V_s) is defined as:

$$A_s = (V_{s2} - V_{s1})/V_s \times 100\%, \quad (6)$$

where V_{s1} and V_{s2} represent the two orthogonally polarized S wave velocities of the mineral, respectively; V_s is aggregate transverse velocity. The results showed that the maximum value for A_s ($A_{s,max}$) of rhodochrosite increased from ~40% at 0.8 GPa to ~48% at 9.7 GPa, while A_p decreased from ~19% to ~16% at the corresponding pressure, the errors of A_p and $A_{s,max}$ were ~0.5% and ~0.9% respectively. The results are abnormal compared with other calcite-type carbonates, whose A_p and A_s are both increased as a function of pressure [6,19,20]. The situations of A_p decreasing and A_s increasing as a function of pressure are also reported in some other minerals, such as orthopyroxene and clinopyroxene [20].

Magnesite is considered as the most important carbon carrier of carbonates in the mantle and its existence is also proved by the occurrence of inclusions in natural diamonds from the deep mantle [29]. Along with magnesite, high pressure phase of rhodochrosite is also proved to be stable at lower mantle pressure condition [8] and considered as a potential carbon carrier in the deep carbon cycle [7]. However, the amount of rhodochrosite is far less than magnesite in the Earth's interior. Magnesite is considered as the major carbon carrier of carbonates in the deep mantle. The contribution of its velocity to the peridotite or eclogite model is within the uncertainty of sound velocity and can be neglected from a
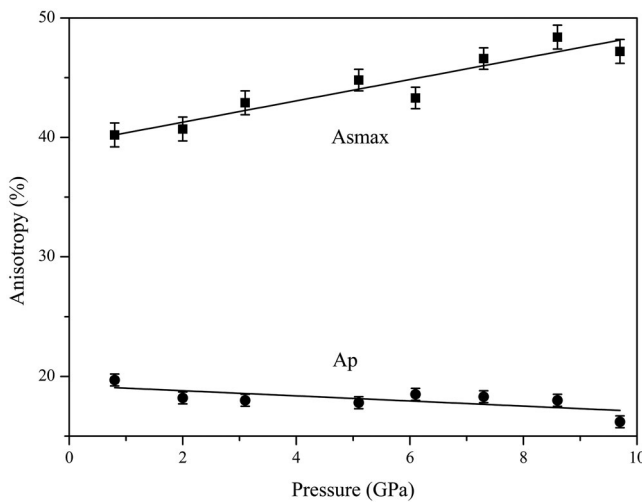

Figure 6. The anisotropy factors for V_p and V_s of rhodochrosite as a function of pressure at ambient temperature.

mineral physics prospective [2,20]. Therefore, it is reasonable to consider that the contribution of rhodochrosite to the velocities of peridotite or eclogite model can be neglected. Nevertheless, the anisotropy factor $A_{s,max}$ of $MnCO_3$ (∼40–48% anisotropy) is much larger than that of $(Mg,Fe)CO_3$ and other major upper mantle minerals, which may be as a potential feature to detect the carbonated region in the Earth's interior [2,20].

4. Conclusion

The sound velocity properties of single-crystal rhodochrosite were determined at high pressure and ambient temperature by Brillouin scattering. Relevant elastic properties were firstly derived and exhibited. The anisotropy factor of rhodochrosite for the maximum of transverse wave anisotropy $A_{s,max}$ increases and the longitudinal wave anisotropy A_p decreases as a function of pressure, which differs from other calcite-type carbonates. These characteristics improve the knowledge of the calcite-type carbonates.

Disclosure statement

No potential conflict of interest was reported by the authors.

References

[1] Dasgupta R, Hirschmann MM. The deep carbon cycle and melting in Earth's interior. Earth Planet Sci Lett. 2010;298:1–13.
[2] Sanchez-Valle C, Ghosh S, Rosa AD. Sound velocities of ferromagnesian carbonates and the seismic detection of carbonates in eclogites and the mantle. Geophys Res Lett. 2011;38(24): L24315-1–L24315-6.
[3] Hazen RM, Downs RT, Jones AP, et al. Carbon mineralogy and crystal chemistry. Rev Mineral Geochem. 2013;75(1):7–46.
[4] Oganov AR, Glass CW, Ono S. High pressure phases of $CaCO_3$: crystal structure prediction and experiment. Earth Planet Sci Lett. 2006;241:95–103.
[5] Oganov AR, Ono S, Ma Y, et al. Novel high pressure structures of $MgCO_3$, $CaCO_3$ and CO_2 and their role in Earth's lower mantle. Earth Planet Sci Lett. 2008;273:38–47.
[6] Stekiel M, Nguyen-Thanh T, Chariton S, et al. High pressure elasticity of $FeCO_3$-$MgCO_3$ carbonates. Phys Earth Planet In. 2017;271:57–63.
[7] Boulard E, Goncharov AF, Blanchard M, et al. Pressure-induced phase transition in $MnCO_3$ and its implications on the deep carbon cycle. J Geophys Res. 2015;120(6):4069–4079.

[8] Liu J, Caracas R, Fan D, et al. High pressure compressibility and vibrational properties of (Ca, Mn)CO$_3$. Am Mineral. 2016;101:2723–2730.

[9] Farfan GA, Boulard E, Wang S, et al. Bonding and electronic changes in rhodochrosite at high pressure. Am Mineral. 2013;98:1817–1823.

[10] Chen CC, Lin CC, Liu LG, et al. Elasticity of single-crystal calcite and rhodochrosite by Brillouin spectroscopy. Am Mineral. 2001;86:1525–1529.

[11] Christensen NI. Elastic properties of polycrystalline magnesium, iron, and manganese carbonates to 10 kilobars. J Geophys Res. 1972;77(2):369–372.

[12] Mao HK, Xu JA, Bell PM. Calibration of the ruby pressure gauge to 800 kbar under quasi-hydrostatic conditions. J Geophys Res. 1986;91(B5):4673.

[13] Zha CS, Duffy TS, Downs RT, et al. Sound velocity and elasticity of single-crystal forsterite to 16 GPa. J Geophys Res. 1996;101:17535–17545.

[14] Murakami M, Asahara Y, Ohishi Y, et al. Development of in situ Brillouin spectroscopy at high pressure and high-temperature with synchrotron radiation and infrared laser heating system: application to the Earth's deep interior. Phys Earth Planet In. 2009;174:282–291.

[15] Sanchez-Valle C, Mantegazzi D, Bass JD, et al. Equation of state, refractive index and polarizability of compressed water to 7 GPa and 673 K. J Chem Phys. 2013;138:054505.

[16] Yoneda A, Song M. Frequency domain analysis of ultrasonic velocity: An alternative bond effect correction constraining bond properties. J Appl Phys. 2005;97:024908.

[17] Whitfield CH, Brody EM, Bassett WA. Elastic moduli of NaCl by Brillouin scattering at high pressure in a diamond anvil cell. Rev Sci Instrum. 1976;47:942–947.

[18] Lin CC. Elasticity of calcite: thermal evolution. Phys Chem Miner. 2013;40:157–166.

[19] Fu S, Yang J, Lin JF. Abnormal elasticity of single-crystal magnesiosiderite across the spin transition in Earth's lower mantle. Phys Rev Lett. 2017;118:036402.

[20] Yang J, Mao Z, Lin JF, et al. Single-crystal elasticity of the deep-mantle magnesite at high pressure and temperature. Earth Planet Sci Lett. 2014;392:292–299.

[21] Biedermann N, Winkler B, Speziale S, et al. Single-crystal elasticity of SrCO$_3$ by Brillouin spectroscopy. High Press Res. 2017;37(2):181–192.

[22] Liu LG, Chen CC, Lin CC, et al. Elasticity of single-crystal aragonite by Brillouin spectroscopy. Phys Chem Miner. 2005;32:97–102.

[23] Chen PF, Chiao LY, Huang PH, et al. Elasticity of magnesite and dolomite from a genetic algorithm for inverting Brillouin spectroscopy measurements. Phys Earth Planet In. 2006;155:73–86.

[24] Merlini M, Hanfland M, Gemmi M. The MnCO$_3$-II high pressure polymorph of rhodocrosite. Am Mineral. 2015;100:2625–2629.

[25] Tan JC, Civalleri B, Lin CC, et al. Exceptionally low shear modulus in a prototypical imidazole-based metal-organic framework. Phys Rev Lett. 2012;108, 095502(095501)-095502(095506).

[26] Rao MN, Chaplot SL, Goel P, et al. Lattice dynamics in rhodochrosite, MnCO$_3$. Appl Phys A: Mater. 2002;74:s1152–s1154.

[27] Simon AR, Angel RJ. High pressure behaviour and equation of state of calcite, CaCO$_3$. Contrib Mineral Petr. 1999;134:102–106.

[28] Meister R, Peselnick L. Variational method of determining effective moduli of polycrystals with tetragonal symmetry. J Appl Phys. 1966;37(11):4121–4125.

[29] Wang AL, Pasteris JD, Meyer HO, et al. Magnesite-bearing inclusion assemb-lage in natural diamond. Earth Planet Sci Lett. 1996;141:293–306.